Available online at www.sciencedirect.com
SCIENCE DIRECT®
Journal of Solid State Chemistry 177 (2004) 2855–2861
JOURNAL OF SOLID STATE CHEMISTRY
http://elsevier.com/locate/jssc

Synthesis and crystal structure of the novel $Pb_5Sb_2MnO_{11}$ compound

Artem M. Abakumov,[a,*] Marina G. Rozova,[a] Pavel S. Chizhov,[a] Evgeny V. Antipov,[a] Joke Hadermann,[b] and Gustaaf Van Tendeloo[b]

[a] *Department of Chemistry, Moscow State University, Leninskie Gory, Moscow 119992, Russia*
[b] *EMAT, University of Antwerp (RUCA), Groenenborgerlaan 171, B-2020 Antwerp, Belgium*

Received 8 January 2004; received in revised form 21 April 2004; accepted 25 April 2004

Abstract

The new $Pb_5Sb_2MnO_{11}$ compound was synthesized using a solid-state reaction in an evacuated sealed silica tube at 650°C. The crystal structure was determined ab initio using a combination of X-ray powder diffraction, electron diffraction and high-resolution electron microscopy ($a = 9.0660(8)$ Å, $b = 11.489(1)$ Å, $c = 10.9426(9)$ Å, S.G. *Cmcm*, $R_I = 0.045$, $R_P = 0.059$). The $Pb_5Sb_2MnO_{11}$ crystal structure represents a new structure type and it can be considered as quasi-one-dimensional, built up of chains running along the *c*-axis and consisting of alternating $Mn^{+2}O_7$ capped trigonal prisms and Sb_2O_{10} pairs of edge sharing $Sb^{+5}O_6$ octahedra. The chains are joined together by Pb atoms located between the chains. The Pb^{+2} cations have virtually identical coordination environments with a clear influence of the lone electron pair occupying one vertex of the PbO_5E octahedra. Electronic structure calculations and electron localization function distribution analysis were performed to define the nature of the structural peculiarities. $Pb_5Sb_2MnO_{11}$ exhibits paramagnetic behavior down to $T = 5$ K with Weiss constant being nearly equal to zero that implies lack of cooperative magnetic interactions.

Keywords: $Pb_5Sb_2MnO_{11}$; Preparation; Crystal structure; Electron microscopy

1. Introduction

Recently, we reported the synthesis and structural investigation of $(Sb_{1-x}Pb_x)_2(Mn_{1-y}Sb_y)O_4$ ($0.0 \leqslant x \leqslant 0.608$, $0.0 \leqslant y \leqslant 0.372$) solid solutions (Abakumov et al., submitted to J. Solid State Chem., 2003) with the Sb_2MnO_4-derived structure [1,2]. Upon variation of the cation composition above the upper limit of the homogeneity range (i.e., for large Pb content), a new phase with a C-centered orthorhombic unit cell was observed as an admixture. In this contribution we report the preparation, crystal structure and chemical bonding analysis for this $Pb_5Sb_2MnO_{11}$ compound which possesses an original structure and represents a new structure type.

2. Experimental

The samples were prepared in evacuated sealed silica tubes using solid-state reaction of various mixtures of different starting materials. Commercial (Reakhim, "chemically pure" purity grade, AlfaAesar, 99.99%) PbO, Pb_3O_4, PbO_2, Sb_2O_3, MnO, Mn_2O_3 and MnO_2 were used as initial reagents. The amounts of initial reagents taken according to the required cation ratio, oxygen content and overall sample weight of 0.5–0.6 g, were intimately mixed under acetone and pressed into pellets. The pellets were placed into alumina crucibles to prevent interaction with the ampoule walls and sealed under dynamic vacuum of 10^{-3} mbar into silica tubes with a diameter of 12 mm and a length of 60 mm. The samples were annealed at 650°C for 50–150 h with intermediate regrinding and then finally furnace cooled.

Phase analysis and cell parameter determination were performed using X-ray powder diffraction with a focusing Guinier-camera FR-552 ($CuK\alpha_1$-radiation, Ge was used as an internal standard) and a Philips X'pert

*Corresponding author. Fax: +7-95-939-47-88.
E-mail address: abakumov@icr.chem.msu.ru (A.M. Abakumov).

0022-4596/$ - see front matter © 2004 Elsevier Inc. All rights reserved.
doi:10.1016/j.jssc.2004.04.047

diffractometer (Cu$K\alpha$-radiation, reflection geometry, proportional counter). X-ray powder diffraction data for crystal structure determination were collected on a STADI-P diffractometer (Cu$K\alpha_1$-radiation, curved Ge monochromator, transmission mode, linear PSD). CSD program package was used for ab initio structure determination and the Rietveld refinement from powder X-ray diffraction data [3]. The profile reliability factors were calculated after background intensity subtraction.

Samples for electron microscopy were made by grinding the powder sample in ethanol and depositing it on a holey carbon grid. Electron diffraction (ED) patterns and EDX spectra were obtained using a Philips CM20 electron microscope. EDX analysis was performed with Pb($M\alpha$), Sb(Lα) and Mn(Kα) lines, using Pb_2MnO_4 and Sb_2MnO_4 as standards. High-resolution electron microscopy (HREM) observations were made on a JEOL 4000EX instrument, having a point-to-point resolution of 1.7 Å. Image simulations were carried out with the MacTempas software.

Magnetic susceptibility measurements were performed with a Quantum Design SQUID magnetometer (MPMS-XL) in a 1000 Oe applied field in the temperature range of 5–385 K.

Electronic structure calculation and electron localization function (ELF) analysis were carried out with the TB-LMTO-ASA program [4]. The Barth–Hedin LDA functional [5] with additional Langreth–Mehl–Hu nonlocal part was used for exchange-correlation treating in the SCF calculation. The k-space integration was performed by the standard tetrahedron method using 14 k-points within the irreducible Brillouin zone. The basis set consisted of 6s, 6p-orbitals for Pb, 5s, 5p-orbitals for Sb, 4s, 4p, 3d-orbitals for Mn and 2p-orbitals for O. 6d, 5f-orbitals for Pb, 5d, 4f-orbitals for Sb, 3s, 3d-orbitals for O were treated using a down-folding technique. The spin-polarized case was considered; all Mn sites were treated as equivalent. The ELF distribution was calculated using the intrinsic procedure of the TB-LMTO-ASA program complex.

3. Results and discussion

3.1. Sample preparation

The target compound was prepared starting from the $4PbO_2 + PbO + MnO_2 + Sb_2O_3$ mixture. After annealing at 650°C for 50 h, the $Pb_5Sb_2MnO_{11}$ phase with a large amount of the $Pb_2Sb_2O_7$ pyrochlore, PbO and Mn_3O_4 was obtained. The subsequent annealing for 50 h after regrinding the sample significantly improved the sample quality leaving only a small amount of the pyrochlore admixture (the intensity of the strongest peak is $I_{rel} = 4.0\%$) and traces of metallic Pb. $Pb_5Sb_2MnO_{11}$ has a yellow-greenish color. The X-ray powder pattern of $Pb_5Sb_2MnO_{11}$ was indexed on an orthorhombic lattice with cell parameters $a = 9.0660(8)$Å, $b = 11.489(1)$Å, $c = 10.9426(9)$Å. The observed $h\,k\,l$: $h + k = 2n$ and $h\,0\,l$: $h, l = 2n$ reflection conditions suggest *Cmcm* as the highest space group for this compound. Syntheses starting from combinations of other oxides of constituent metals (e.g., $PbO_2 + 3Pb_3O_4 + 2MnO + 2Sb_2O_3$ or $3PbO_2 + 7PbO + Mn_2O_3 + 2Sb_2O_3$) that provide the same total stoichiometry also allow to prepare samples with $Pb_5Sb_2MnO_{11}$ as a main constituent, but with a larger amount of admixture phases (up to 7–9% of the pyrochlore, PbO and Mn_3O_4). Deviation from the stoichiometric composition by decreasing the Pb content by 10 at% or increasing the oxygen content up to $Pb_5Sb_2MnO_{11.2}$ result in a drastic increase of the amount of impurity phases and yield the pyrochlore phase as the main phase in the samples. Increasing the Mn content ("$Pb_{4.5}Sb_2Mn_2O_{12}$" sample), however, allows to suppress the formation of the pyrochlore admixture, but results in the appearance of 3–4% of Mn_3O_4 and an unknown phase. The unit cell parameters of $Pb_5Sb_2MnO_{11}$ remain the same within the range of two standard deviations for all samples, which indicates that the compound composition does not depend on the choice of the initial reagents and synthesis conditions. The cation composition of the $Pb_5Sb_2MnO_{11}$ phase was confirmed by EDX analysis in the transmission electron microscope performed at 12 points on four different crystallites. The cation ratio Pb:Sb:Mn = 5.03(7):1.98(7):0.99(3) was found to be very close to the nominal one.

3.2. Crystal structure and ELF distribution analysis

The crystal structure of $Pb_5Sb_2MnO_{11}$ was solved ab initio from X-ray powder diffraction data. The integral intensities of the reflections over the angular range 10–80° 2θ were determined by profile fitting and then used for the direct structure solution. The *Cmcm* space group was assumed for the initial structure model. The analysis of the resulting electron density map revealed the positions of the Pb atoms. The atomic coordinates of the Sb, Mn and oxygen atoms were found by a sequence of difference Fourier syntheses. Prior to the Rietveld refinement of the obtained structure model the impacts of six impurity peaks of Mn_3O_4 and the unknown phase were subtracted from the raw data using their fitted profiles since they did not overlap with the peaks from the main phase. The refinement was carried out in an isotropic approximation for the atomic displacement parameters. Preferred orientation along the [110] direction was taken into account using the March–Dollase function. After sequential iterations, a good agreement between the experimental and calculated profiles was achieved: $R_I = 0.045$, $R_P = 0.059$, $R_{wP} = 0.052$. An

attempt to refine the crystal structure with the $Cmc2_1$ space group did not improve reliability factors and resulted in strong correlations between the atomic coordinates of Pb atoms, which are symmetrically related in the *Cmcm* space group. The crystallographic parameters, atomic coordinates and the most relevant interatomic distances for $Pb_5Sb_2MnO_{11}$ are listed in Tables 1–3. The observed, calculated, and difference X-ray diffraction patterns are shown in Fig. 1.

To our knowledge, the $Pb_5Sb_2MnO_{11}$ structure has no analogues, and therefore it represents a new structure type. The crystal structure of $Pb_5Sb_2MnO_{11}$ can be considered as quasi-one-dimensional, built up of chains of manganese-oxygen and antimony-oxygen polyhedra running along the *c*-axis and joined together by Pb atoms located between the chains (Fig. 2). Each chain consists of Sb_2O_{10} units built up of two SbO_6 octahedra with the O2, O3 and O4 atoms as vertices linked by the common O2–O2 edge. The Sb_2O_{10} units are located above each other along the chain direction so the two neighboring units are mirror-related. Two O2 and four O3 atoms form a trigonal prismatic cavity between these two units, which is filled by Mn cations. The coordination environment of the Mn atoms is completed up to CN = 7 by an O1 atom which forms a cap above one rectangular face of the trigonal prism. The tendency of the SbO_6 octahedra to share common edges forming Sb_2O_{10} pairs ($K_3Sb_5O_{14}$ [6], $MSbO_3$, (M = Li, K, Ag) [7–9], MSb_2O_6 (M = Co, Cu) [10,11]), chains (Na_3SbO_4 [12]), layers ($CdSb_2O_6$ [13], MSb_2O_6 (M = Mn, Ca) [14,15], $TlSbO_3$ [16]) or frameworks ($K_2Sb_4O_{11}$ [6]) is a characteristic feature of Sb^{+5} cations. The average interatomic distances $\langle d(Sb-O)\rangle = 2.000$ Å and $\langle d(Mn-O)\rangle = 2.322$ Å are in agreement with the ionic radii of the Sb^{+5} and Mn^{+2} cations ($r(Sb^{+5}) = 0.75$ Å for CN = 6, $r(Mn^{+2}$, CN = 7) $\approx 1/2(r(Mn^{+2}$, CN = 6) + $r(Mn^{+2}$, CN = 8)) = 1.02 Å, $r(O^{-2}) = 1.26$ Å). The coordination environments of the Pb1, Pb2 and Pb3 atoms are virtually identical. They can be represented as a distorted tetragonal pyramid where the apical vertex is formed by O1 atoms, and the square base consists of either four O4 atoms (for Pb1) or two O3 and two O4 ones (for Pb2 and Pb3) (Fig. 3). The lead atoms are not located inside the pyramids, but are shifted outside, away from the O1 atom. One may assume that such a distortion can be understood if the influence of the lone electron pair of the Pb^{+2} cations is taken into account. The lone pair completes the coordination environment of the Pb atoms to a PbO_5E (E = lone electron pair) octahedron and is directed along the apical axis of the

Table 1
Selected parameters from Rietveld refinement of X-ray powder data for $Pb_5Sb_2MnO_{11}$

Formula	$Pb_5Sb_2MnO_{11}$
Space group	*Cmcm*
a (Å)	9.06282(5)
b (Å)	11.48250(6)
c (Å)	10.94024(6)
Z	4
Cell volume (Å^3)	1139.08(3)
Calculated density (g/cm^3)	5.721
2θ range, step (deg)	$10 \leqslant 2\theta \leqslant 110$, 0.01
Number of reflections	431
Refinable parameters	27
Preferred orientation parameter and axis	1.428(7), [110]
Reliability factors:	
R_I, R_P, R_{wP}	0.045, 0.059, 0.052

Table 2
Positional and atomic displacement parameters of atoms for $Pb_5Sb_2MnO_{11}$

Atom	Position	*x*/*a*	*y*/*b*	*z*/*c*	B_{iso} (Å^2)
Pb1	4*c*	0	0.99957(8)	1/4	1.45(2)
Pb2	8*g*	0.27674(7)	0.21715(6)	3/4	1.57(2)
Pb3	8*f*	0	0.21923(7)	0.52277(5)	1.32(2)
Sb	8*e*	0.3257(1)	0	1/2	1.04(3)
Mn	4*c*	1/2	0.0841(3)	1/4	1.31(8)
O1	4*c*	0	0.202(1)	3/4	0.4(3)
O2	8*f*	1/2	0.0635(7)	0.5974(7)	0.7(2)
O3	16*h*	0.3330(7)	0.1401(5)	0.3918(5)	1.1(2)
O4	16*h*	0.1839(6)	0.0729(4)	0.6116(5)	0.8(2)

Table 3
Selected interatomic distances for $Pb_5Sb_2MnO_{11}$ (Å)

Pb1–O1	2.317(13) × 1	Sb–O2	2.041(5) × 2
Pb1–O4	2.401(6) × 4	Sb–O3	1.999(5) × 2
Pb2–O1	2.514(1) × 1	Sb–O4	1.961(6) × 2
Pb2–O3	2.467(6) × 2	Sb–Sb	3.159(1) × 1
Pb2–O4	2.396(5) × 2	Mn–O1	2.454(13) × 1
Pb3–O1	2.494(1) × 1	Mn–O2	2.379(8) × 2
Pb3–O3	2.403(6) × 2	Mn–O3	2.261(6) × 4
Pb3–O4	2.559(5) × 2		

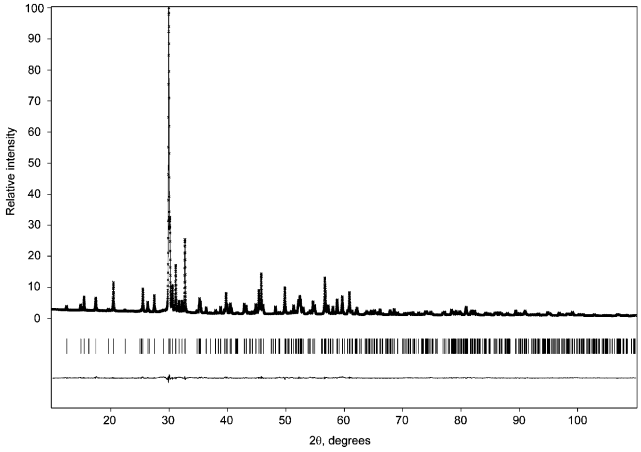

Fig. 1. The experimental, calculated and difference X-ray diffraction patterns for $Pb_5Sb_2MnO_{11}$.

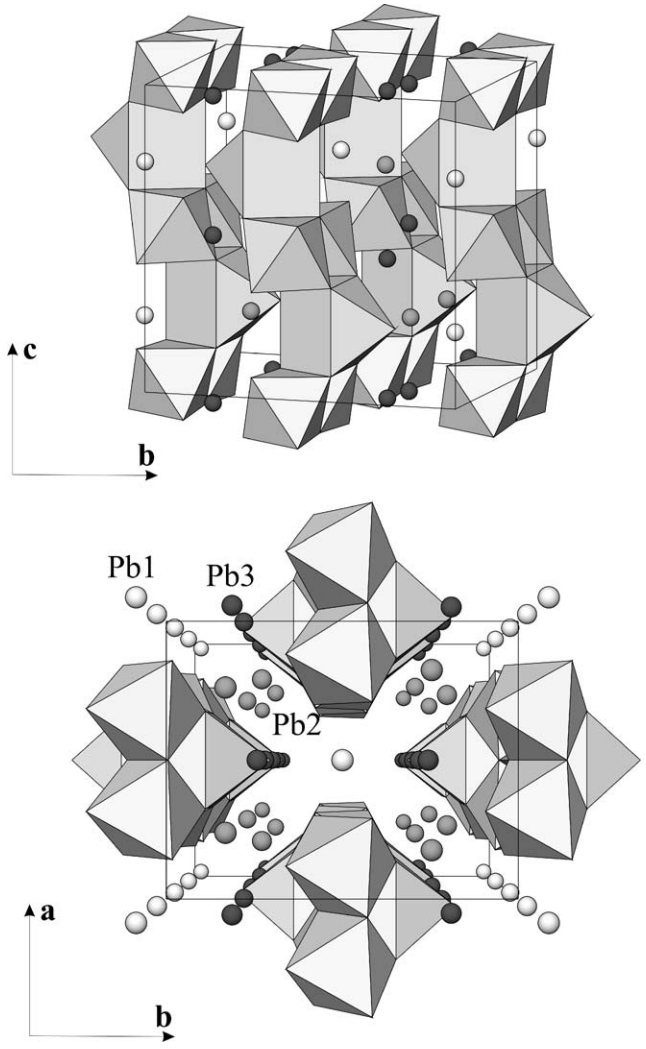

Fig. 2. [100] and [001] projections of the $Pb_5Sb_2MnO_{11}$ crystal structure. Sb atoms are located inside the octahedra, Mn atoms are inside the capped trigonal prisms. White, gray and black spheres represent Pb1, Pb2 and Pb3 atoms, respectively.

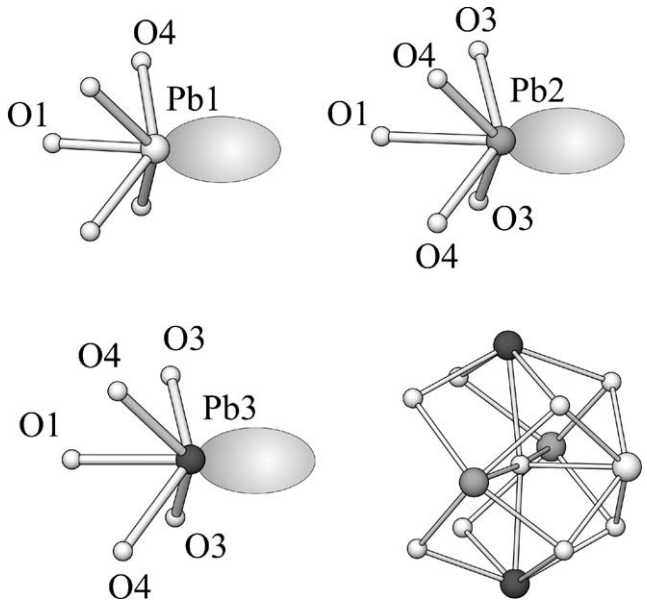

Fig. 3. Coordination environment of the Pb1, Pb2 and Pb3 cations in the $Pb_5Sb_2MnO_{11}$ crystal structure. Orientation of the lone electron pairs of the Pb cations is shown. The right bottom figure represents the Pb_5O_9 cluster consisting of PbO_5E octahedra.

octahedron away from the O1 atom. The location of the O3 and O4 atoms then follows the valence shell electron pair repulsion model assuming the requirement of a larger space for the lone pair in the vicinity of the Pb atom than for a bonding pair. The PbO_5E octahedra around one Pb1, two Pb2 and two Pb3 atoms are joined together by common faces forming a Pb_5O_9 cluster with the O1 atom at the center and the lone pairs directed away from the cluster center (Fig. 3). The location of these clusters in the unit cell is shown in Fig. 4. The orientation of lone pair clouds with respect to the crystal axes can be revealed from this figure: the lone pair clouds are aligned along [010] for Pb1, [100] for Pb2 and [001] for Pb3. The assumption about the lone electron pairs, localized on the Pb atoms, was further proved by the analysis of the ELF distribution, which confirms the nature of the coordination peculiarities in the $Pb_5Sb_2MnO_{11}$ structure. Thus, an area of strong electron localization, or, in other words, the lone electron pair (Fig. 5, $\eta = 0.85$ isosurface), exists near the open corner of the PbO_5E octahedra. The absence of an electron localization near Sb and between two Sb atoms of the Sb_2O_{10} units allows to suggest that Sb in the Sb_2O_{10} units has the formal oxidation number $+5$ and there is no Sb–Sb bonding even in spite of the relatively short Sb–Sb distance of 3.159(1)Å. After analysis of DOS, projected DOS (Fig. 6) and moments on the atoms one can conclude that Mn^{2+} is strongly spin-polarized, or, in other words, there is high-spin d^5 configuration of Mn^{2+} ion in this compound. Fermi level in this case lies just above the occupied non-bonding e_g orbitals of octahedrally coordinated Mn^{2+}. All other atoms are practically spin-unpolarized. The substance in this case is a semiconductor with the estimated band gap of about 0.88 eV.

The experimentally determined coordination environments, the $Pb_5Sb_2MnO_{11}$ composition and the ELF distribution analysis suggest the formal valences of Pb, Sb and Mn cations to be equal to $+2$, $+5$ and $+2$, respectively. The coexistence of Mn^{+2} and Sb^{+5} in the same structure was also found before in $MnSb_2O_6$ [14] and $Mn_2Sb_2O_7$ [17] oxides. The valences were also verified by BVS calculations which give the values of $+2.40$ for Pb1, $+2.03$ for Pb2, $+2.01$ for Pb3, $+5.14$ for Sb and $+1.70$ for Mn. For the Pb2, Pb3 and Sb atoms the calculated BVS values agree well with the proposed valence distribution, but the bond valence sum is overestimated for Pb1 and underestimated for Mn. The most probable explanation is that the X-ray powder

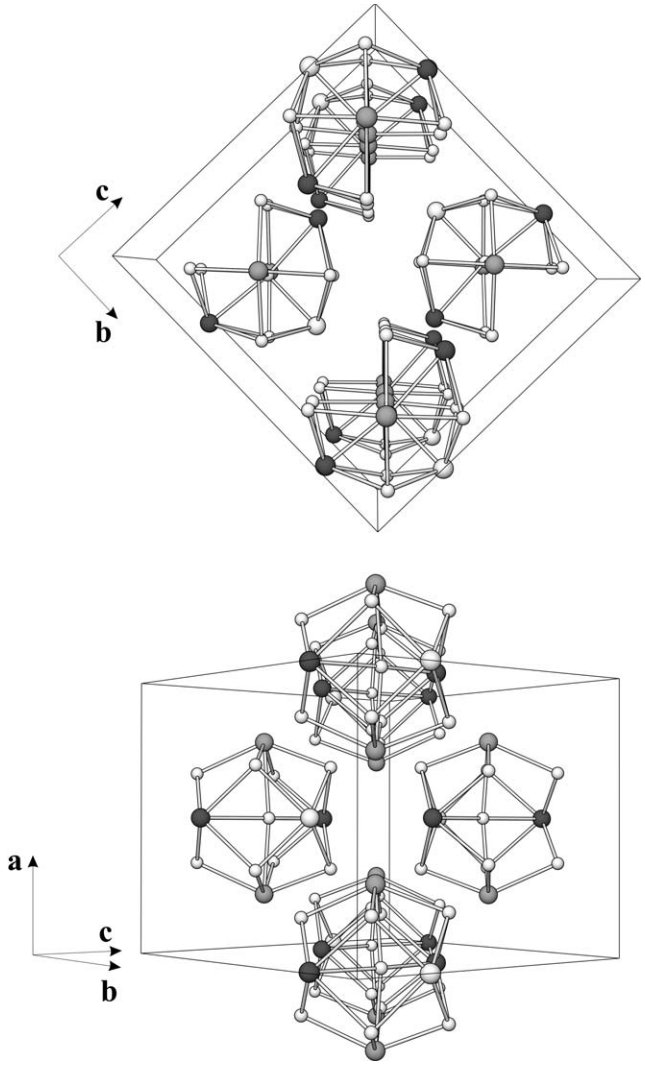

Fig. 4. Location of the Pb_5O_9 clusters in the $Pb_5Sb_2MnO_{11}$ crystal structure.

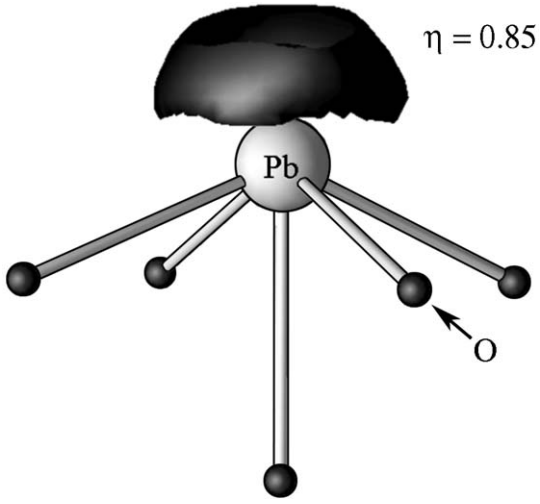

Fig. 5. ELF distribution near Pb in PbO_5E octahedra ($\eta = 0.85$ isosurface, Pb2 is taken as an example, the Pb1 and Pb3 atoms exhibit similar features).

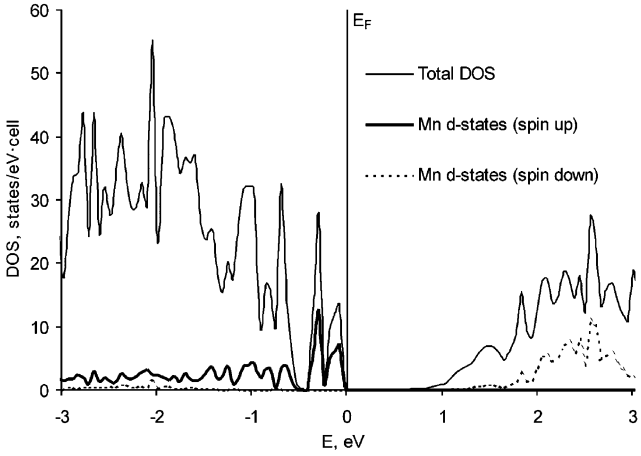

Fig. 6. Total DOS and Mn-*d*-spin up/spin down projected DOS curves near Fermi level.

refinement does not allow to determine precisely the *y*/*b* coordinate for the O1 atom. Indeed, shifting the O1 atom from the 0, 0.202, 0.75 position towards 0, 0.235, 0.75 allows to obtain the BVS values of +2.04 and +1.99 for the Pb1 and Mn cations, respectively and almost does not change the BVS values for the Pb2 and Pb3 cations. However, the atomic coordinate for the O1 atom always converges to $y/b = 0.202$. One might expect that the refinement of the positions of the oxygen atoms in the presence of such heavy scatterers as Pb cannot be very precise in the case of conventional X-ray powder diffraction, and the refinement from neutron diffraction data will be helpful in this case.

3.3. Electron microscopy analysis

ED patterns for $Pb_5Sb_2MnO_{11}$ taken along the most prominent zone axes are shown in Fig. 7. All patterns can be indexed completely on an orthorhombic lattice with the unit cell parameters determined using X-ray powder diffraction. The presence of the $h\,k\,l$: $h+k=2n$ and $h\,0\,l$: $h,l=2n$ reflection conditions is clearly visible on the $[010]^*$, $[001]^*$ and $[101]^*$ ED patterns. The forbidden $0\,0\,l$: $l\neq 2n$ reflections on the $[100]^*$ and $[110]^*$ patterns are caused by multiple diffraction as was confirmed by tilting the crystal around the c^*-axis. No other extinction conditions or extra reflections were observed, which confirms the chosen unit cell and the *Cmcm* space symmetry.

The HREM images taken along the [100] and [110] zone axes are shown in Fig. 8. Oxygen columns and cation columns are projected separately viewed along the [100] direction. At this thickness and defocus value the nearly square pattern of the bright dots represents the columns of oxygen atoms. The inserted theoretical image, calculated at $\Delta_f = -200$ Å and $t = 110$ Å using

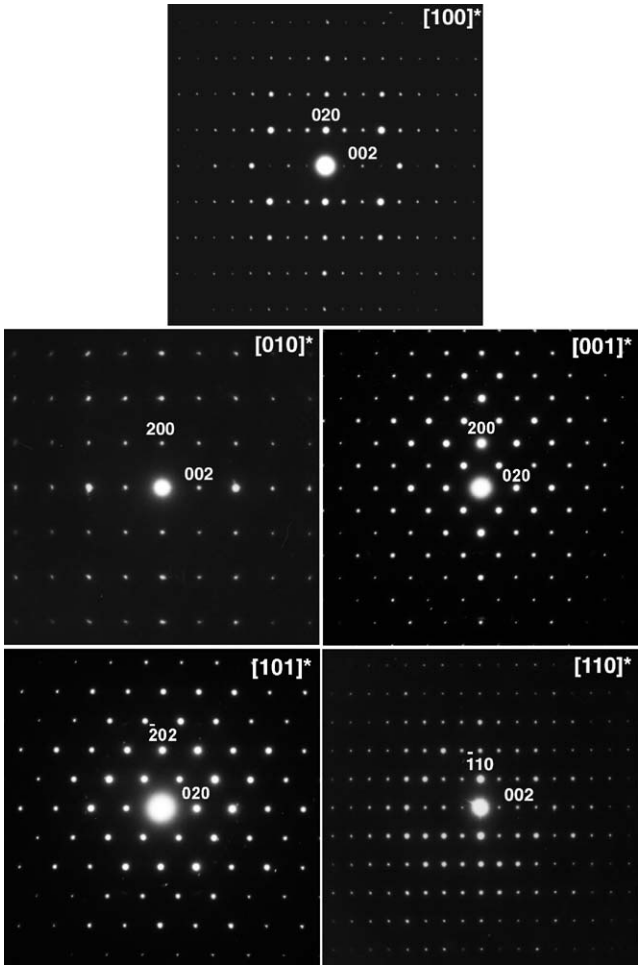

Fig. 7. [100]*, [010]*, [001]*, [101]* and [110]* ED patterns for the $Pb_5Sb_2MnO_{11}$ phase.

the atomic coordinates as determined from X-ray powder diffraction, reproduces well the square pattern of bright dots and the intensity variation in the dot rows along the *c*-axis. The [110] HREM image shows the projection of the cation columns as a centered rectangular bright dot pattern. The theoretical image calculated with $\Delta_f = 300$ Å and $t = 40$ Å is in good agreement with the experimental one. The HREM images exhibit a faultless structure and no extended defects are found.

3.4. Magnetic properties

The temperature dependence of dc susceptibility revealed paramagnetic behavior (Fig. 9). A fit of the inverse susceptibility to the Curie–Weiss law yielded the effective moment of 5.81 μ_B, in agreement with a theoretical spin-only value for the Mn^{+2} (d^5, high spin) of 5.92 μ_B. The Weiss constant (θ) is zero within the error, indicating the absence of significant magnetic interactions between Mn^{+2} spins. This behavior is not unexpected because magnetic ions (Mn^{+2}) in the chains

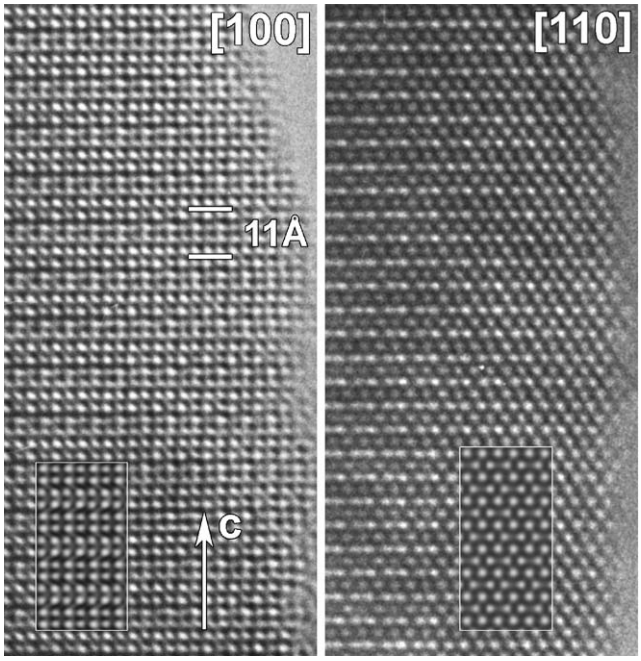

Fig. 8. The [100] and [110] HREM images of $Pb_5Sb_2MnO_{11}$. Insets show the theoretical images calculated at $\Delta_f = -200$ Å and $t = 110$ Å (for the [100] zone axis) and at $\Delta_f = 300$ Å and $t = 40$ Å (for the [110] zone axis).

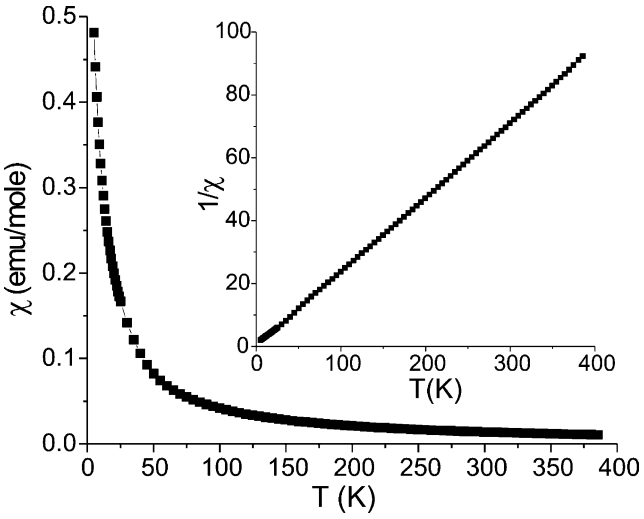

Fig. 9. Temperature dependence of the dc magnetic susceptibility of $Pb_5Sb_2MnO_{11}$. Inset shows inverse susceptibility vs. T plot.

are well separated by non-magnetic entities (Sb_2O_{10} octahedral clusters).

Acknowledgments

The authors are grateful to M. Lobanov and M. Greenblatt for the magnetic measurements. The work was supported in part by the program IAP V-1 of the Belgium government. Acknowledgment is made to the

donors of the American Chemical Society Petroleum Research Fund for partial support of this research (project 38459-AC5). A.M.A. is grateful to INTAS for the Fellowship grant for Young Scientists YSF 2002-48. E.V.A. is grateful to Russian Science Support Foundation for the financial support.

References

[1] R. Chater, J.R. Gavarri, J. Solid State Chem. 59 (1985) 123.
[2] H. Fjellvag, A. Kjekshus, Acta Chem. Scand. A 39 (1985) 389.
[3] L.G. Akselrud, Yu.N. Grin, P.Yu. Zavalij, V.K. Pecharsky, V.S. Fundamentsky, in: Thesis report on 12th ECM, Moscow, 1989, p. 155.
[4] O.K. Andersen, O. Jepsen, M. Snob, in: Linearized Band-Structure Method in Electronic Band Structure and its Applications, Lecture Notes in Physics, Springer, Berlin, 1987.
[5] U. von Barth, L. Hedin, J. Phys. C 4 (1964) 1971.
[6] H.Y.P. Hong, Acta Crystallogr. 30 (1974) 945.
[7] J.L. Fourquet, P.A. Gillet, A. Le Bail, Mater. Res. Bull. 24 (1989) 1207.
[8] P. Spiegelberg, Ark. Kemi, Miner. Geol. A 14 (1940) 1.
[9] H.Y.P. Hong, J.A. Kafalas, J.B. Goodenough, J. Solid State Chem. 9 (1974) 345.
[10] J.N. Reimers, J.E. Greedan, C.V. Stager, R. Kremer, J. Solid State Chem. 83 (1989) 20.
[11] E.-O. Giere, A. Brahimi, H.J. Deiseroth, D. Reinen, J. Solid State Chem. 131 (1997) 263.
[12] B. Schwedes, R. Hoppe, Z. Anorg. Allg. Chem. 393 (1972) 136.
[13] A. Castro, I. Rasines, M.C. Sanches-Martos, P. Garcia-Casado, Powder Diffr. 3 (1988) 219.
[14] H. Vincent, X. Turrillas, I. Rasines, Mater. Res. Bull. 22 (1987) 1369.
[15] B.G. De Boer, R.A. Young, A. Sakthivel, Acta Crystallogr. 50 (1994) 476.
[16] M. Bouchama, M. Tournoux, Rev. Chim. Miner. 12 (1975) 80.
[17] H.G. Scott, Zeit. Kristallogr. 190 (1990) 41.